




Article

Assembly of Imidazolyl-Substituted Nitronyl Nitroxides into Ferromagnetically Coupled Chains

Vasily Romanov ¹, Irina Bagryanskaya ^{1,2}, Nina Gritsan ^{3,4} , Dmitry Gorbunov ^{3,4}, Yulia Vlasenko ⁵, Mehman Yusubov ⁵, Elena Zaytseva ^{1,2} , Dominique Luneau ^{6,*} and Evgeny Tretyakov ^{1,2,*} 

¹ N. N. Vorozhtsov Institute of Organic Chemistry, 9 Ac. Lavrentiev Avenue, Novosibirsk 630090, Russia; romanov@nioch.nsc.ru (V.R.); bagryan@nioch.nsc.ru (I.B.); elena@nioch.nsc.ru (E.Z.)

² Department of Natural Sciences, Novosibirsk State University, 2 Pirogova Str., Novosibirsk 630090, Russia

³ Institute of Chemical Kinetics and Combustion, 3 Institutskaya Str., Novosibirsk 63009, Russia; gritsan@kinetics.nsc.ru (N.G.); personal.daemon@gmail.com (D.G.)

⁴ Physics Department, Novosibirsk State University, 2 Pirogova Str., Novosibirsk 630090, Russia

⁵ Research School of Chemistry & Applied Biomedical Sciences, Tomsk Polytechnic University, Tomsk 634050, Russia; vlasenkoiuliia16@gmail.com (Y.V.); yusubov@mail.ru (M.Y.)

⁶ Université Claude Bernard Lyon-1, Campus de La Doua, 69622 Villeurbanne Cedex, France

* Correspondence: dominique.luneau@univ-lyon1.fr (D.L.); tretyakov@nioch.nsc.ru (E.T.); Tel.: +33-472-43-1418 (D.L.); +7-383-330-9171 (E.T.)

Received: 21 March 2019; Accepted: 18 April 2019; Published: 23 April 2019



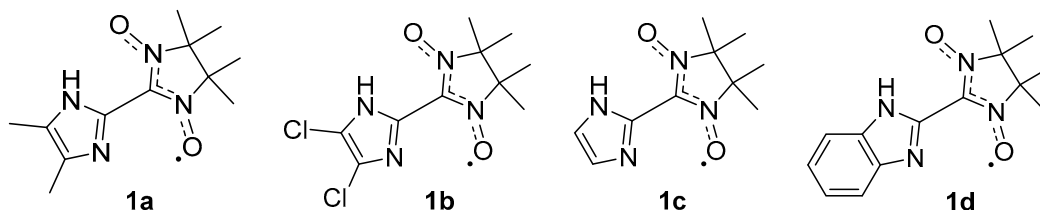
Abstract: New nitronyl nitroxides, namely, 2-(4,5-dimethylimidazol-2-yl)- and 2-(4,5-dichloroimidazol-2-yl)-4,4,5,5-tetramethyl-4,5-dihydro-1*H*-imidazol-3-oxide-1-oxyl, were prepared in crystalline form. According to single-crystal X-ray data, intra- and intermolecular hydrogen bonds are formed between NH groups of the imidazole cycles and O atoms of the nitroxide moieties. The intermolecular H-bonds contribute to the alignment of molecules into chains along the *a*-axis; this alignment causes short intrachain contacts between O and C atoms carrying spin density of opposite signs. Such an arrangement of nitroxides induces ferromagnetic intrachain interactions ($J \approx 10 \text{ cm}^{-1}$) between neighboring radicals.

Keywords: nitronyl nitroxides; imidazole; crystal structure; hydrogen bonding; exchange interaction; density functional theory

1. Introduction

Long-range ferromagnetic ordering has been and is the main target of many scientists looking for organic magnets [1]. The key point in the design of pure organic magnetic materials is the assembly of the building blocks (spin-carriers) so that they interact ferromagnetically. This is a fundamental problem because the relationship between the relative orientation of the radicals in a crystal and the magnetic properties of the paramagnetic crystals is complicated. The reason is that the magnetic behavior of monoradicals results from a combination of the magnetic intermolecular interactions generated by the individual contacts, which depends on all the functional groups present in the paramagnetic molecule [2]. This fact makes it impossible to perform magneto–structural analysis of all available data on purely organic paramagnets. It is more fruitful, we believe, to concentrate on a series of compounds having closely related structures tending to form similar first crystalline motifs. These motifs are formed due to the strongest intermolecular contacts among which hydrogen bonds are the most predictable, and simultaneously they have an important role in the propagation of ferromagnetic interactions in organic molecular solids [3–12]. Keeping all this in mind, we performed the synthesis and characterization of new nitroxide radicals **1a,b** carrying an imidazole ring substituted

at positions 4 and 5 with methyl groups or chloro-atoms (Scheme 1). It was found that the introduction of substituents into the imidazole ring leads to a change in the first crystalline motif or primary structure of **1a,b** as compared to **1c**. As a result, the dominating strong antiferromagnetic exchange interactions inherent in **1c** changed to the ferromagnetic ones observed in **1a,b**. Of note, benzo-annulation of the imidazole ring in **1d** has the same effect, thus, ensuring similarities of magnetic properties between **1a,b** and **1d**.



Scheme 1. Structures of imidazolyl- and benzimidazolyl-substituted nitronyl nitroxides **1a–d**.

2. Materials and Methods

2.1. General Procedures

4,5-Dichloro-2-hydroxymethylimidazole [13] and *N,N'*-(2,3-dimethylbutane-2,3-diyl)-bis(hydroxyl-amine) (BHA) and its sulfate [14] were synthesized as reported earlier. All the solvents were of reagent quality, and all commercial reagents were used without additional purification. The reactions were monitored by thin-layer chromatography on silica gel 60 F₂₅₄ aluminum sheets from Merck. The yields are given for pure substances obtained after recrystallization.

¹H NMR spectra were recorded at 400 MHz on Bruker AVANCE III HD; chemical shifts are reported in parts per million (ppm) and referenced relative to the solvent. Infrared (IR) spectra were obtained from KBr pellets by means of a Bruker VECTOR 22 infrared spectrometer. Melting points were determined on a Boetius melting point apparatus. Microanalyses were performed using a Carlo Erba 1106 analyzer. Mass spectra were recorded on a Finnigan MAT-8200 instrument by the electron impact ionization technique (70 eV).

Electron paramagnetic resonance (EPR) spectra were registered in a diluted and oxygen-free toluene solution at 295 K at the concentrations of 10^{−4} M by means of a commercial Bruker X-Band (9 GHz) spectrometer, Elecsys E540. To determine isotropic *g*-factors (*g*_{iso}), we simultaneously recorded X-band continuous-wave EPR spectra of two samples placed in separate sample tubes (Finland trityl as a reference and the radical being analyzed, and, thus, obtained the target *g*_{iso} value relative to the known *g*_{iso} of Finland trityl). The simulations of the solution EPR lines were carried out using the software package Easy Spin, which is available at <http://www.easypin.org>.

2.2. Synthetic Procedures

2.2.1. 4,4,5,5-Tetramethyl-2-(4,5-dimethyl-1*H*-imidazolyl)-4,5-dihydro-1*H*-imidazole-3-oxide-1-oxyl (**1a**)

Hydrate of *N,N'*-(2,3-dimethylbutane-2,3-diyl)bis(hydroxylamine) sulfate (1056 mg, 4 mmol) was added at room temperature to a stirred solution of 4,5-dimethyl-1*H*-imidazole-2-carbaldehyde (496 mg, 4 mmol) in water (5 mL). The reaction mixture was stirred for 1 h at room temperature, and then the solution was kept at ca. 5 °C for 48 h. The precipitate was filtered off and washed with cold water on a filter. The resulting pale white powder was dissolved in ethanol (10 mL), and MnO₂ (1740 mg, 20 mmol) was added. The reaction mixture was stirred for 3 h at room temperature and filtered. The mother solution was concentrated to a volume of ca. 2 mL. Then, it was diluted with benzene (10 mL) and placed onto a column. The column was eluted with ethyl acetate, and a bluish violet fraction was collected; this fraction was evaporated. The solvent was distilled off, the residue was ground with hexane, and the solvent decanted. Yield: 763 mg (76%); blue crystals; m.p. 91–93 °C; IR (KBr): $\tilde{\nu}$ = 461 w, 486 w, 542 m, 604 w, 629 w, 646 w, 663 w, 696 m, 717 m, 763 w, 831 vw, 870 m, 972 w,

1001 w, 1024 m, 1135 s, 1176 s, 1195 s, 1267 m, 1342 vs, 1367 s, 1388 s, 1436 vs, 1558 s, 1591 w, 1627 w, 1687 w, 2613 w, 2861 m, 2941 m, 2991 m, 3062 m, 3168 s, 3192 s·cm⁻¹; UV/Vis (EtOH): λ^{\max} (ϵ) = 312 vs (19960), 377 w (4660), 642 vw (640), 708 vw nm (620 mol⁻¹·dm³·cm⁻¹) (Supplementary Materials Figures S4 and S5); elemental analysis calcd (%) for C₁₂H₁₉N₄O₂ (251.15): C 57.35, H 7.62, N 22.29; found C 57.42, H 7.64, N 22.28.

2.2.2. 1-Tosyloxy-1-oxo-1*H*-1*λ*5-benzo[d][1,2]iodoxol-3-one (IBX-OTs)

This compound was prepared by treating 2-iodoxybenzoic acid (IBX) with *p*-TsOH·H₂O in acetic anhydride according to a published procedure [15]. A mixture of IBX (2.73 g, 9.75 mmol), *p*-TsOH·H₂O (5.55 g, 29.25 mmol, 3.0 equiv), and acetic anhydride (37.5 mL) was stirred at room temperature. Formation of a clear colorless solution was observed after 30 to 40 min of stirring, and then a white microcrystalline precipitate started to form. After the mixture was stirred for an additional 4 h, the precipitate was filtered and washed on filter with a mixture (40 mL) of Et₂O and Ac₂O (20:1) and dried in vacuum (0.01 mbar) at room temperature for 24 h to obtain 4.01 g (91% yield) of 1-tosyloxy-1-oxo-1*H*-1*λ*5-benzo[d][1,2]iodoxol-3-one (IBX-OTs) monohydrate, as a white, microcrystalline solid; m.p. 118–119 °C (dec.); ¹H NMR ([D₆]DMSO, 25 °C): δ = 8.16 (d, *J* = 8.0 Hz, 1H), 8.01 (m, 2H), 7.85 (t, *J* = 7.6 Hz, 1H), 7.48 (d, *J* = 8.0 Hz, 2H), 7.13 (d, *J* = 8.0 Hz, 2H), 2.29 ppm (s, 3H). ¹H NMR (CD₂Cl₂-CF₃COOH 10:1, 25 °C): δ = 8.44 (d, *J* = 8.5 Hz, 1H), 8.29 (d, *J* = 7.5 Hz, 1H), 8.17 (t, *J* = 7.5 Hz, 1H), 7.98 (t, *J* = 7.5 Hz, 1H), 7.55 (d, *J* = 8.0 Hz, 2H), 7.24 (d, *J* = 8.0 Hz, 2H), 2.40 ppm (s, 3H) (Supplementary Materials Figure S1).

2.2.3. 4,5-Dichloro-1*H*-imidazole-2-carbaldehyde

The oxidation of (4,5-dichloro-1*H*-imidazol-2-yl)methanol was carried out according to a procedure described elsewhere [16]. To a suspension of (4,5-dichloro-1*H*-imidazol-2-yl)methanol (0.752 g, 4.5 mmol) in CH₂Cl₂ (45 mL), IBX-OTs·H₂O (2.441 g, 1.2 equiv) was added with stirring at room temperature. The reaction mixture was stirred for 1 h until full conversion of the starting material (monitored by thin-layer chromatography and gas chromatography with mass spectrometry). The analytically pure product was isolated by filtration of the reaction mixture through a short silica gel column with dichloromethane as an eluent. The solvent was removed under reduced pressure at room temperature. The product was obtained as a white solid; yield: 520 mg (70%); ¹H NMR ([D₆]DMSO, 25 °C): δ = 9.46 ppm (s, 1H) (Figure S2).

2.2.4. 4,4,5,5-Tetramethyl-2-(4,5-dichloro-1*H*-imidazolyl)-4,5-dihydro-1*H*-imidazole-3-oxide-1-oxyl (**1b**)

N,N'-(2,3-dimethylbutane-2,3-diyl)bis(hydroxylamine) (1480 mg, 10 mmol) was added at room temperature to a stirred solution of 4,5-dichloro-1*H*-imidazole-2-carbaldehyde (1650 mg, 10 mmol) in dimethylformamide (DMF, 20 mL). The reaction mixture was stirred for 48 h at 30 °C under Ar, and then DMF was removed under a stream of air. The resulting pale white powder was dissolved in ethanol (50 mL), and MnO₂ (4.5 g, 50 mmol) was added. The reaction mixture was stirred for 3 h at room temperature and filtered. The mother solution was concentrated to a volume of ca. 10 mL and placed onto an Al₂O₃ column. The latter was subjected to elution with ethanol, and a bluish violet fraction was collected; the fraction was evaporated. The solvent was distilled off, the residue was ground up with hexane, and the solvent decanted. Yield: 760 mg (26%); blue crystals; m.p. 86–88 °C; IR (KBr): $\tilde{\nu}$ = 455 w, 507 vw, 543 m, 576 w, 611 w, 649 w, 705 w, 719 vw, 738 w, 761 w, 831 vw, 870 m, 962 vw, 972 vw, 1026 m, 1138 m, 1175 m, 1217 m, 1240 w, 1296 w, 1332 s, 1353 s, 1373 s, 1403 vs, 1427 vs, 1450 s, 1510 m, 1548 m, 1579 w, 1621 w, 1629 w, 1677 w, 1768 w, 2618 w, 2794 m, 2989 m, 3425 m·cm⁻¹; UV/Vis (EtOH): λ^{\max} (ϵ) = 323 vs (16800), 370 w (2980), 628 vw nm (580 mol⁻¹·dm³·cm⁻¹) (Figures S6 and S7); elemental analysis calcd (%) for C₁₀H₁₃N₄O₂ (291.04): C 41.11, H 4.49, N 24.27; found C 41.03, H 4.45, N 24.28.

2.3. Single-Crystal X-Ray Diffraction Analysis

X-ray crystallographic analyses of the crystals were carried out on a Bruker Kappa Apex II CCD diffractometer using phi and omega scans of narrow (0.5°) frames with Mo K α radiation ($\lambda = 0.71073$ Å) and a graphite monochromator (Table 1). The structures were solved by direct methods in the SHELX-97 software [17] and refined by the full-matrix least-squares method against all F^2 in anisotropic approximation by means of the SHELXL-2014/7 software suite [18]. The hydrogen atom positions were calculated via the riding model. Absorption corrections were applied by the empirical multiscan method in the SADABS software [19]. The obtained crystal structures were analyzed for short contacts between nonbonded atoms in PLATON [20,21] and MERCURY [22].

CCDC 1830809 and 1830810 contain the crystallographic data for **1a** and **1b**, respectively. These data can be obtained free of charge via <http://www.ccdc.cam.ac.uk/cgi-bin/catreq.cgi>, or from the Cambridge Crystallographic Data Centre, 12 Union Road, Cambridge CB2 1EZ, UK; fax: (+44) 1223 336 033; or e-mail: deposit@ccdc.cam.ac.uk.

Table 1. X-ray diffraction data for nitronyl nitroxides **1a,b**.

Compound	1a	1b
Empirical formula	C ₁₂ H ₁₉ N ₄ O ₂	C ₁₀ H ₁₃ N ₄ O ₂ Cl ₂
Formula weight	251.31	292.14
Temperature, K	296(2)	296(2)
Wavelength, Å	0.71073	0.71073
Crystal system	Orthorhombic	Orthorhombic
Space group	<i>Pbca</i>	<i>Pbca</i>
Unit cell dimensions <i>a</i> , Å	8.7454(4)	8.7195(5)
<i>b</i> , Å	15.4621(8)	15.460(1)
<i>c</i> , Å	19.852(1)	19.551(1)
Volume, Å ³ ; <i>Z</i>	2684.4(2); 8	2635.5(3); 8
Density (calcd.), mg·m ⁻³	1.244	1.473
Abs. coefficient, mm ⁻¹	0.087	0.493
F(000)	1080	1208
Crystal size, mm ³	0.06 × 0.06 × 0.9	0.02 × 0.06 × 0.40
θ range for data collection, °	4.0–25.0	2.6–26.0
Index ranges	–10 ≤ <i>h</i> ≤ 10, –18 ≤ <i>k</i> ≤ 18, –23 ≤ <i>l</i> ≤ 23	–10 ≤ <i>h</i> ≤ 10, –19 ≤ <i>k</i> ≤ 19, –24 ≤ <i>l</i> ≤ 24
Reflections collected	34103	29738
Independent reflections	2365 R(int) = 0.063	2603 R(int) = 0.104
Completeness to θ , %	99.5	99.8
Data / restraints / parameters	2365/0/169	2603/0/167
Goodness-of-fit on F^2	1.01	1.00
Final <i>R</i> indices $I > 2\sigma(I)$	$R_1 = 0.0481$, $wR_2 = 0.1338$	$R_1 = 0.0448$, $wR_2 = 0.0863$
Final <i>R</i> indices (all data)	$R_1 = 0.0584$, $wR_2 = 0.1461$	$R_1 = 0.0978$, $wR_2 = 0.1049$
Largest diff. peak / hole, e·Å ⁻³	0.22/–0.25	0.24/–0.22

2.4. Magnetic Measurements

Magnetic susceptibility data (at 2–300 K) on polycrystalline samples were determined using an MPMS-XL SQUID magnetometer of Quantum Design (San Diego, CA, USA) in a 0.1 T applied magnetic field. The magnetization isotherm was recorded between 0 and 5 T. All data were corrected for a contribution of the sample holder and diamagnetism of the samples estimated via Pascal's constants [23].

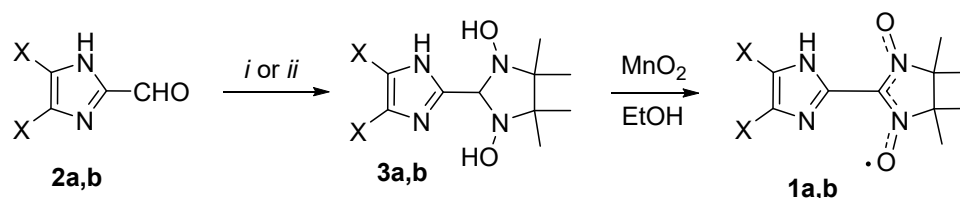
2.5. Computational Details

The spin densities, hyperfine coupling constants and g-tensors were calculated at the density functional theory level. To calculate parameters J of the exchange interaction ($\hat{H} = -2J\hat{S}_1\hat{S}_2$) between the radicals, the spin-unrestricted broken-symmetry (BS) approach [24] was chosen. The J values were calculated via the formula $J = -\frac{E_{HS}-E_{LS}}{S^2_{HS}-S^2_{LS}}$, where E_{HS} is the energy of the triplet state of the radical pair, and E_{LS} denotes the energy of the broken-symmetry singlet state [24]. In all cases, the $\langle S^2 \rangle_{HS}$ values were close to 2.0, and $\langle S^2 \rangle_{LS}$ to 1.0. All the calculations for the X-ray structure geometries were performed at the UB3LYP/def2-TZVP level of theory [25–27] using Orca 4.0.1.2 software [28].

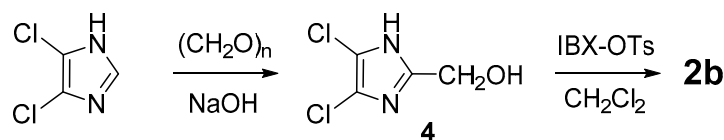
3. Results and Discussion

Nitronyl nitroxides **1a** and **1b** were synthesized according to the classical scheme [29] involving the condensation of corresponding aldehydes **2a,b** with 2,3-bis(hydroxyamino)-2,3-dimethylbutane (BHA) followed by the oxidation of dehydroadducts **3a,b** (Scheme 2). The condensation reaction of dimethyl-derivative **2a** with BHA·H₂SO₄ was carried out in water. In the case of dichloro-derivative **2b**, these conditions were found to be inapplicable and led to the formation of a mixture of products; the desired 1,3-dihydroxyimidazolidine **3b** was successfully prepared only by interaction of **2b** with BHA in DMF. In contrast to other oxidants (PbO₂, NaIO₄), only MnO₂ led to the oxidation of **3a,b** to nitronyl nitroxides **1a,b** with high yields.

Conditions providing effective oxidation of hydroxymethyl-derivative **4** could also be of interest to the organic chemists' community. Among different oxidants (pyridinium chlorochromate and SeO₂) that we tested, the only effective reagent appeared to be 1-tosyloxy-1-oxo-1*H*-1*λ*5-benzo[d][1,2]iodoxol-3-one (IBX-OTs), which afforded aldehyde **2b** with a high yield (~70%, Scheme 3). Aldehyde **2b**, as compared with **2a**, has limited stability and should be applied to the condensation with BHA immediately after preparation.



Scheme 2. Synthesis of nitronyl nitroxides **1a** and **1b** (X = Me, *i*: *N,N'*-(2,3-dimethylbutane-2,3-diyl)-bis(hydroxyl-amine) (BHA)·H₂SO₄, water; X = Cl, *ii*: BHA, dimethylformamide (DMF)).



Scheme 3. Effective synthesis of 4,5-dichloro-imidazole-2-carbaldehyde **2b**.

In a diluted ($C \approx 10^{-4}$ M) and oxygen-free toluene solution, the electron paramagnetic resonance (EPR) spectra of **1a,b** contained clear-cut isotropic five-line patterns at $g = 2.0057$ (Figure S3). Such a five-line spectrum originates from the interaction of the unpaired electron with the two equivalent nitrogen nuclei of the imidazoline moiety. Relative intensities of the lines followed the expected 1:2:3:2:1 ratio. The best fit to the observed EPR spectra was achieved with the following parameters, which are fairly well consistent with the calculations at the UB3LYP/def2-TZVP level (in parentheses): $A_{N1} = A_{N3} = 0.76$ (0.50) mT, $g_{iso} = 2.0057$ (2.0068) for **1a**, and $A_{N1} = A_{N3} = 0.75$ (0.50) mT, $g_{iso} = 2.0057$ (2.0068) for **1b**.

Crystallization of compounds **1a,b** from a mixture of CH₂Cl₂ with hexane gave well-shaped dark blue crystals (Figures S8 and S9). Crystals of **1a** are stable and can be stored at least for a half year at +5 °C in a fridge. On the contrary, nitroxide **1b** is unstable and undergoes decomposition with the formation of a colorless product after 2 months. The structures of radicals **1a,b** were successfully confirmed by single-crystal X-ray diffraction (Figure 1). General crystallographic data for these compounds are summarized in Table 1. According to the X-ray diffraction analysis, nitroxides **1a,b** are isostructural and crystallize in the orthorhombic *Pbca* space group. The N–O (1.279–1.284 Å) and C3–N (1.338–1.345 Å) bond lengths are unexceptional and similar to those previously described for nitronyl nitroxide free radicals [30]. The nitronyl nitroxide moiety is not symmetrical due to the participation of one NO group in H-bonding leading to slight elongation of both NO and adjacent NC bonds. In **1a** and **1b**, the dihedral angle between the planes of the imidazole cycle and nitronyl nitroxide moiety is 20.0(2)° and 17.5(3)°, respectively.

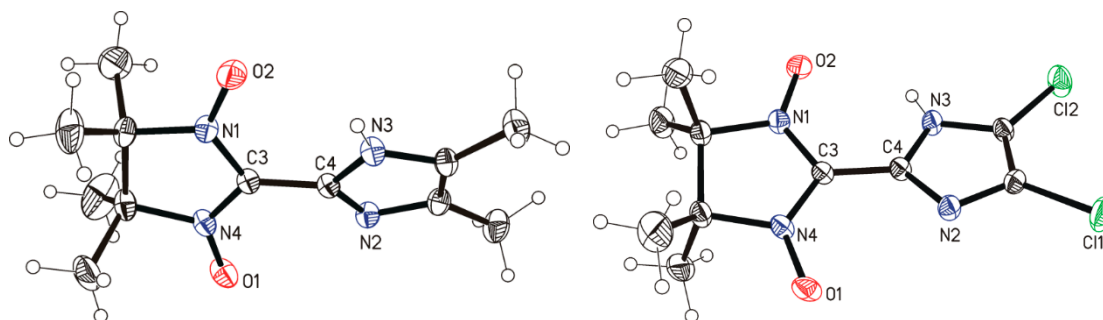


Figure 1. Molecular structures of **1a** and **1b** (ellipsoids of thermal oscillations at 30% probability).

In solid **1a** and **1b**, NH groups of the imidazole ring participate in the formation of intramolecular and intermolecular hydrogen bonds of the NH ... O type. The latter causes formation of one-dimensional (1D) infinite chains of molecules along axis *a* with distances N ... O 2.874(2) for **1a** and 2.811(3) Å for **1b** (Figure 2). Inside the chains, there are short intermolecular contacts between O atoms of one molecule and C3 atoms of an adjacent molecule, 3.145(2) and 3.050(3) Å, respectively, in **1a** and **1b** (note that a normal O...C contact is 3.35 Å [31]). The aforementioned contacts NH ... O are slightly shorter than those between O atoms [3.291(2) Å in **1a**, and 3.125(3) Å in **1b**].

Surprisingly, the crystal packing of nitroxide radicals **1a,b** is different from that of unsubstituted 2-imidazol-2-yl nitronyl nitroxide **1c**. In solid **1c**, the nitroxide radicals are aligned into chains by means of intermolecular H-bonds of the N–H ... N type (2.873(5)Å) [7], and the nitroxide O atoms are not involved in the formation of H-bonds [7]. At the same time, the crystal packing of nitroxide radicals **1a,b** resembles that of 2-benzimidazol-2-yl nitronyl nitroxide **1d** [7]. The only difference is that in **1d**, the corresponding distances NH ... O and O ... C3 are slightly longer than those in **1a,b** and equal to 2.86(3) and 3.13(3) Å, respectively. This is likely because there is greater hindrance caused by the fused benzene cycle than by the two methyl (**1a**) or chlorine (**1b**) substituents at the fourth and fifth positions of the imidazole ring.

Because the crystal structure motif of **1a,b,d** is different from that of **1c**, one would expect essentially different magnetic behaviors. In solid state **1c**, antiferromagnetic exchange interactions dominate with a large singlet–triplet gap of $2J \approx -123 \text{ cm}^{-1}$ as estimated using the Bleaney–Bowers model [7]. For **1a** at room temperature, the product of magnetic susceptibility and temperature (χT) is $0.36 \text{ emu}\cdot\text{K}\cdot\text{mol}^{-1}$, which is close to the expected value ($0.375 \text{ emu}\cdot\text{K}\cdot\text{mol}^{-1}$) for noninteracting radicals. This value sharply increases with the decreasing temperature and reaches a maximum of $0.6 \text{ emu}\cdot\text{K}\cdot\text{mol}^{-1}$ at 5 K. With further lowering of the temperature, χT decreases to $0.37 \text{ emu}\cdot\text{K}\cdot\text{mol}^{-1}$ at 2 K. This behavior indicates the dominance of ferromagnetic interactions between the radicals although weaker antiferromagnetic interactions exist and manifest themselves in the decay of χT at $T < 5 \text{ K}$ (Figure 3).

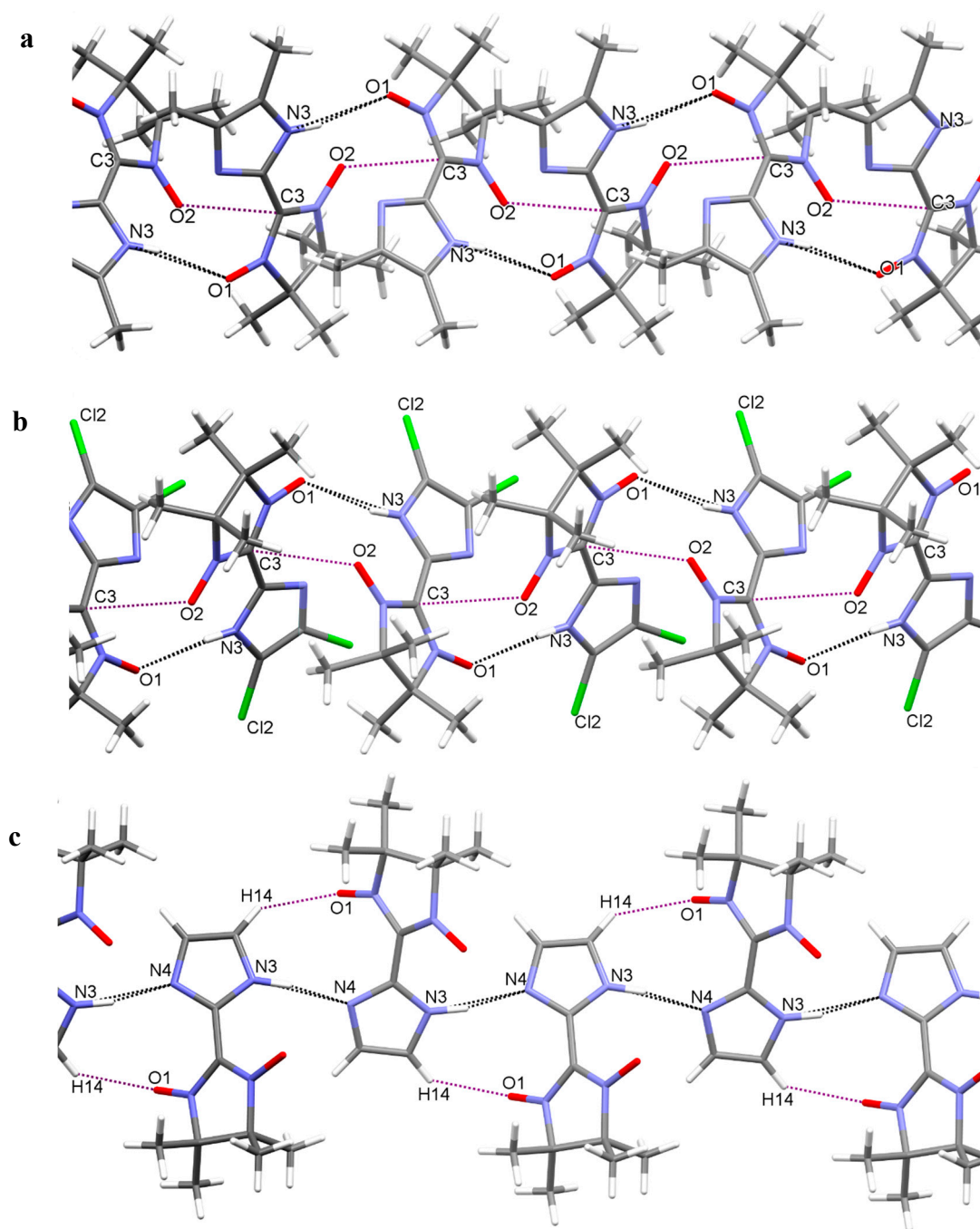


Figure 2. Fragments of the H-bonded chains in **1a** (a), **1b** (b), and **1c** (c). Short contacts O2... C3 and O1... H14 are indicated by purple dotted lines.

The $1/\chi$ temperature dependence above 20 K is fitted well by the Curie–Weiss law ($\frac{1}{\chi(T)} = \frac{T-\theta}{C}$) with Curie constant $C = 0.334 \pm 0.001 \text{ emu}\cdot\text{K}\cdot\text{mol}^{-1}$ and Weiss temperature $\theta = 5.4 \pm 0.3 \text{ K}$ (Figure 3, black line). The temperature dependence of χT was fitted to the 1D-Heisenberg ferromagnetic model [32,33] taking into account the weak antiferromagnetic interaction between radicals of neighboring chains in the mean field approximation (1)

$$\chi T = \chi_{1D} T / \left[1 - \frac{\theta'}{T} \right] \quad (1)$$

and in a more rigorous manner (2)

$$\chi T = \frac{\chi_{1D} T}{\left[1 - \frac{zJ'}{2k} \frac{\chi_{1D}}{C}\right]} \quad (2)$$

where C is the Curie constant: $C = \frac{Ng^2\beta^2}{3k} S(S+1) = \frac{Ng^2\beta^2}{4k}$. In the mean field approximation, a good fit was obtained with ferromagnetic coupling constant $J = 7.1 \pm 0.4$ K (or 5.0 ± 0.3 cm⁻¹) and $\theta' = -3.0 \pm 0.2$ K (Figure 3, red curve). Fitting via formula (2) led to $J = 6.8 \pm 0.3$ K (or 4.7 ± 0.2 cm⁻¹) and $J' = -0.55 \pm 0.02$ K. Both results are in fair agreement with the value obtained for **1d** [7].

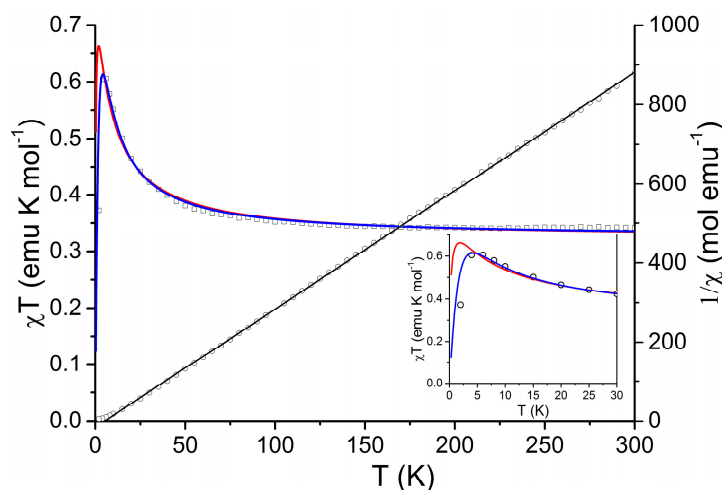


Figure 3. χT and $1/\chi$ versus T plots for **1a**. The straight line corresponds to the best fit of $1/\chi$ (Curie–Weiss law), and the curves correspond to the best fit of χT using the 1D-Heisenberg ferromagnetic model and taking into consideration antiferromagnetic interactions by means of formulas 1 (red curve) and 2 (blue curve).

To confirm the presence of dominant ferromagnetic interactions, the magnetization isotherm for **1a** was determined at 2 K. Figure 4 reveals that the magnetization increases monotonously with the magnetic field, approaching at $H = 5$ T a saturation limit that is close to the expected value for the radicals ($1 \mu_B$). Nevertheless, the magnetization curve is well above the Brillouin function for $S = 1/2$ spins and corresponds better to $S = 2$.

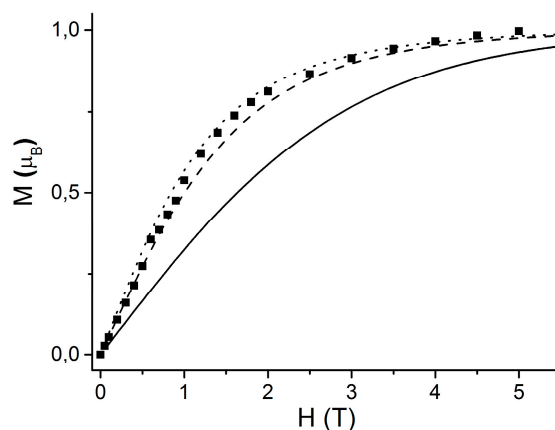


Figure 4. The field dependence of the magnetization of **1a** at 2 K (squares) and Brillouin functions for $S = 1/2$ (solid curve), $S = 3/2$ (dashed curve), and $S = 2$ (dotted curve).

As mentioned above, nitroxide **1b** is prone to decomposition. At room temperature, χT is $0.25 \text{ emu}\cdot\text{K}\cdot\text{mol}^{-1}$, which is much lower than the expected value of $0.375 \text{ emu}\cdot\text{K}\cdot\text{mol}^{-1}$ and indicates a significant degree of decomposition (~33%). Nevertheless, χT steeply increases with the decreasing temperature, also pointing to the dominance of ferromagnetic exchange interactions.

To specify the magnetic motifs of the crystals of compounds **1a–c** and to better understand the origin of the quantitative and qualitative differences, we performed calculations of exchange coupling between radicals via the spin-unrestricted broken-symmetry approach at the UB3LYP/def2-TZVP level (Tables S1–S3). This approach has been demonstrated to well predict the exchange interactions between organic radicals and radical fragments [34,35]. As expected, the spin density distribution is very similar among radicals **1a–c** (Figure 5). As readers can see, significant negative spin density (approximately -0.2) is localized on the carbon atom of the imidazole ring, and for **1c**, the negative density is the highest.

It is obvious that not only the spin density distribution but also the mutual arrangement of radicals influences their exchange interactions. Table 2 represents information about the shortest distances between atoms with high absolute spin density as well as dihedral angle $\angle\text{N1–O2–O1'–N4'}$, which is an estimate of the angle between the planes of the nitronyl nitroxide moieties. Table 2 shows that for **1a,b**, the O2 ... C3 distance is slightly shorter than the O2 ... O1 distance and that the nitronyl nitroxide moieties are far from being parallel. Both features contribute to the predicted moderate ferromagnetic interaction of these radicals ($J \approx 15 \text{ cm}^{-1}$). In the case of radical **1c**, the O2 ... C3 distance is much longer than O2 ... O1, and the arrangement of the nitronyl nitroxide fragments is close to parallel. Both features contribute to a significant antiferromagnetic interaction. Note that calculations satisfactorily (within a factor of 2 to 3) predict both the positive (ferromagnetic) and negative (antiferromagnetic) J values for compounds **1a** and **1c**, respectively. Instability of compound **1b** did not allow us to determine J , although the ferromagnetic character of dominant interactions is consistent with calculations.

Table 2. Contacts O ... O and O ... C3, and the dihedral angles for the neighboring pairs of radicals, calculated values of exchange interaction parameters (J_{calc}) as well as values corresponding to the best fit of experimental temperature dependences of molar magnetic susceptibility for compounds **1a,b** (this study) and **1c** [7].

Compound	1a	1b	1c
R(O2 ... O1), Å	3.292(2)	3.125(3)	3.484(6)
R(O2 ... C3), Å	3.145(2)	3.050(3)	3.702(7)
$\angle\text{N1–O2 ... O1'–N4'}$	118.3(2)	121.6(2)	180.0(5)
$J_{\text{calc}}, \text{cm}^{-1}$	14.6	16.5	−36.7
$J_{\text{exp}}, \text{cm}^{-1}$	5.0 ± 0.3 ^a 4.7 ± 0.2 ^c	^b –	−61.5 –
$J'_{\text{calc}}, \text{d cm}^{-1}$	−0.31, 0.06	−0.27, 0.01	−0.9, −0.06
θ'_{exp}	$−3.0 \pm 0.2$	^b	–
zJ', K	$−0.55 \pm 0.02$	–	–

^a AF interactions were taken into account in the mean-field approximation. ^b These values could only be estimated as $J = 2.9 \pm 0.2 \text{ K}$ and $\theta' = -1.5 \pm 0.1 \text{ K}$ (1D-Heisenberg ferromagnetic model). ^c AF interactions were taken into account using a more rigorous approximation (see text). ^d Calculated parameters (J'_{calc}) of the exchange interactions between radicals of the neighboring chains.



Figure 5. Mulliken atomic spin densities calculated at the UB3LYP/def2-TZVP level of theory for dichloroimidazole- and dimethylimidazole-substituted nitronyl–nitroxide radicals (**1a,b**) and **1c**.

4. Conclusions

In this work, we describe magneto–structural correlations inherent in the whole family of imidazolyl-substituted nitronyl nitroxides to show the influence of a substitution of the imidazole ring on the self-arrangement of the nitronyl nitroxide moieties for the purpose of control over the ferromagnetic alignment of the spins in the solid. We synthesized and investigated new free radicals of nitronyl nitroxides, namely 2-(4,5-dimethylimidazol-2-yl)- and 2-(4,5-dichloroimidazol-2-yl)-4,4,5,5-tetramethyl-4,5-dihydro-1*H*-imidazol-3-oxide-1-oxyl. The crystal structures of the two radicals are isostructural and afford 1D hydrogen-bonded chains of the nitronyl nitroxides. The hydrogen bonds give rise to short intrachain contacts between the oxygen and carbon atoms possessing the opposite signs of spin density. Such an arrangement of nitronyl nitroxides causes a ferromagnetic spin alignment proved by magnetic susceptibility measurements and density functional theory calculations. Comparative analyses of the magneto–structural relations in nitronyl nitroxides without a substituent on the imidazole ring and with a benzimidazol group suggest that substituents at positions 4 and 5 of the imidazole ring may allow for control over the crystal packing to make the nitronyl nitroxide spin-carriers interact ferromagnetically.

Supplementary Materials: The following are available online at <http://www.mdpi.com/2073-4352/9/4/219/s1>, Figures S1 and S2: ¹H NMR spectra of IBX-OTs and 4,5-dichloro-1*H*-imidazole-2-carbaldehyde, Figure S3: EPR spectra of nitronyl nitroxides **1a,b**, Figures S4–S7: IR and UV/Vis spectra of radicals **1a,b**, Figure S8: Calculated and experimental X-ray powder diffractograms for **1a**, Figure S9: Picture of crystals of **1b**, Tables S1–S3: Selected interatomic distances (Å) and angles (°) and parameters of exchange interaction (J_1) calculated at the BS-DFT level for the closest radicals in the FM chains or AFM pairs, for the closest radicals of the neighboring FM chains or between radical from neighboring AFM pairs, and for the next closest radicals of neighboring FM chains or of neighboring AFM pairs for crystals of radicals **1a–c**.

Author Contributions: Conceptualization, E.T. and D.L.; investigation, V.R., I.B., Yu.V., M.Yu., and E.Z.; formal analysis, D.G., and N.G.

Funding: The authors thank the Russian Foundation for Basic Research (RFBR; projects 17-53-150020 and 18-33-00143) and the CNRS collaborative research program (France) with RFBR (PRC 2017-2019 No. 1536) for financial support.

Acknowledgments: The authors thank the Multi-Access Chemical Research Center SB RAS for the spectral and analytical measurements. D.G. acknowledges the Irkutsk Supercomputer Center of SB RAS for support of the computational part of this work.

Conflicts of Interest: The authors declare no conflict of interest.

References

1. Veciana, J.; Iwamura, H. Organic magnets. *MRS Bull.* **2000**, *25*, 41–51. [[CrossRef](#)]

2. Novoa, J.J.; Deumal, M. The mechanism of the through-space magnetic interactions in purely organic molecular magnets. In *π -Electron Magnetism; Structure and Bonding*; Springer: Berlin/Heidelberg, Germany, 2001; Volume 100, pp. 34–60. [[CrossRef](#)]
3. Hernández, E.; Mas, M.; Molins, E.; Rovira, C.; Veciana, J. Hydrogen bonds as a crystal design element for organic molecular solids with intermolecular ferromagnetic interactions. *Angew. Chem. Int. Ed.* **1993**, *32*, 882–884. [[CrossRef](#)]
4. Cirujeda, J.; Hernández-Gasio, E.; Rovira, C.; Stanger, J.-L.; Turek, P.; Veciana, J. Role of hydrogen bonds in the propagation of ferromagnetic interactions in organic molecular solids. Part 1—The p-hydroxyphenyl α -nitronyl aminoxy radical case. *J. Mater. Chem.* **1995**, *5*, 243–252. [[CrossRef](#)]
5. Cirujeda, J.; Ochando, L.E.; Amigó, J.M.; Rovira, C.; Rius, J.; Veciana, J. Structure determination from powder X-ray diffraction data of a hydrogen-bonded molecular solid with competing ferromagnetic and antiferromagnetic interactions: The 2-(3,4-Dihydroxyphenyl)- α -nitronyl nitroxide radical. *Angew. Chem. Int. Ed.* **1995**, *34*, 55–57. [[CrossRef](#)]
6. Veciana, J.; Cirujeda, J.; Rovira, C.; Molins, E.; Novoa, J. Organic ferromagnets. Hydrogen bonded supramolecular magnetic organizations derived from hydroxylated phenyl α -nitronyl nitroxide radicals. *J. Phys.* **1996**, *6*, 1967–1986. [[CrossRef](#)]
7. Naoki, Y.; Munetoshi, I.; Yuichiro, M.; Takanari, K.; Hidenari, I.; Shigeru, O. Unusually Large Magnetic Interactions Observed in Hydrogen-Bonded Nitronyl Nitroxides. *Chem. Lett.* **1997**, *26*, 251–252. [[CrossRef](#)]
8. Poderoso, J.L.; González-Cabello, A.; Jürgens, O.; Vidal-Gancedo, J.; Veciana, J.; Torres, T.; Vázquez, P. Synthesis and magnetic coupling of a bis(nitronyl nitroxide radical derived from 1,2,4-triazole. *Synth. Met.* **2001**, *121*, 1830–1831. [[CrossRef](#)]
9. Lang, A.; Pei, Y.; Ouahab, L.; Kahn, O. Synthesis, crystal structure, and magnetic properties of 5-methyl-1,2,4-triazole-nitronyl nitroxide: A one-dimensional compound with unusually large ferromagnetic intermolecular interactions. *Adv. Mater.* **1996**, *8*, 60–62. [[CrossRef](#)]
10. Nagashima, H.; Hashimoto, N.; Inoue, H.; Yoshioka, N. Coexistence of an antiferromagnetically coupled dimer and isolated paramagnetic spin in 4-azaindol-2-yl nitronyl nitroxide crystal. *New J. Chem.* **2003**, *27*, 805–810. [[CrossRef](#)]
11. Nagashima, H.; Fujita, S.; Inoue, H.; Yoshioka, N. Metamagnetic behavior observed in purely organic 5-azaindol-2-yl nitronyl nitroxide brick-wall architecture. *Cryst. Growth Des.* **2004**, *4*, 19–21. [[CrossRef](#)]
12. Romanov, V.E.; Bagryanskaya, I.Y.; Gorbunov, D.E.; Gritsan, N.P.; Zaytseva, E.V.; Luneau, D.; Tretyakov, E.V. A crystallographic study of a novel tetrazolyl-substituted nitronyl nitroxide radical. *Crystals* **2018**, *8*, 334. [[CrossRef](#)]
13. Amini, M.; Golabchifar, A.A.; Dehpour, A.R.; Pirali, H.M.; Shafiee, A. Synthesis and calcium channel antagonist activity of new 1,4-dihydropyridine derivatives containing dichloroimidazolyl substituents. *Arzneimittelforschung* **2002**, *52*, 21–26. [[CrossRef](#)]
14. Ovcharenko, V.I.; Fokin, S.V.; Rey, P. A Thorough investigation of the synthetic problems of vic-bis-hydroxylamine—The precursor of Ullman’s nitroxides. *Mol. Cryst. Liq. Cryst.* **1999**, *334*, 109–119. [[CrossRef](#)]
15. Yusubov, M.S.; Svitich, D.Y.; Yoshimura, A.; Nemykin, V.N.; Zhdankin, V.V. 2-Iodoxybenzoic acid organosulfonates: Preparation, X-ray structure and reactivity of new, powerful hypervalent iodine(V) oxidants. *Chem. Commun.* **2013**, *49*, 11269–11271. [[CrossRef](#)] [[PubMed](#)]
16. Yusubov, M.S.; Postnikov, P.S.; Yusubova, R.Y.; Yoshimura, A.; Jürjens, G.; Kirschning, A.; Zhdankine, V.V. 2-Iodoxybenzoic acid tosylates: The alternative to Dess–Martin periodinane oxidizing reagents. *Adv. Synth. Catal.* **2017**, *359*, 3207–3216. [[CrossRef](#)]
17. Sheldrick, G.M. *SHELX-97, Programs for Crystal Structure Analysis (Release 97-2)*; University of Göttingen: Göttingen, Germany, 1997.
18. Sheldrick, G.M. Crystal structure refinement with SHELXL. *Acta Cryst. Sect. C Struct. Chem.* **2015**, *71*, 3–8. [[CrossRef](#)]
19. *SADABS, v. 2008-1*; Bruker AXS: Madison, WI, USA, 2008.
20. Spek, A.L. *PLATON, a Multipurpose Crystallographic Tool (Version 10M)*; Utrecht University: Utrecht, The Netherlands, 2003.
21. Spek, A.L. Single-crystal structure validation with the program PLATON. *J. Appl. Crystallogr.* **2003**, *36*, 7–13. [[CrossRef](#)]

22. Macrae, C.F.; Edgington, P.R.; McCabe, P.; Pidcock, E.; Shields, G.P.; Taylor, R.; Towler, M.; van de Stree, J. Mercury: Visualization and analysis of crystal structures. *J. Appl. Crystallogr.* **2006**, *39*, 453–457. [[CrossRef](#)]
23. Pascal, P. Recherches magnétochimiques (premier memoire). *Ann. Chim. Phys.* **1910**, *19*, 5–70.
24. Soda, T.; Kitagawa, Y.; Onishi, T.; Takano, Y.; Shigeta, Y.; Nagao, H.; Yoshioka, Y.; Yamaguchi, K. Ab Initio computations of effective exchange integrals for H–H, H–He–H and Mn₂O₂ complex: Comparison of broken-symmetry approaches. *Chem. Phys. Lett.* **2000**, *319*, 223–230. [[CrossRef](#)]
25. Becke, A.D. Density-functional thermochemistry III. The role of exact exchange. *J. Chem. Phys.* **1993**, *98*, 5648–5652. [[CrossRef](#)]
26. Lee, C.; Yang, W.; Parr, R.G. Development of the Colle-Salvetti correlation-energy formula into a functional of the electron density. *Phys. Rev. B* **1988**, *37*, 785–789. [[CrossRef](#)]
27. Weigend, F.; Ahlrichs, R. Balanced basis sets of split valence, triple zeta valence and quadruple zeta valence quality for H to Rn: Design and assessment of accuracy. *Phys. Chem. Chem. Phys.* **2005**, *7*, 3297–3305. [[CrossRef](#)]
28. Neese, F. The ORCA program system. *Wires Comput. Mol. Sci.* **2012**, *2*, 73–78. [[CrossRef](#)]
29. Ullman, E.F.; Osiecki, J.H.; Boocok, D.G.B.; Darcy, R. Studies of stable free radicals. X. Nitronyl nitroxide monoradicals and biradicals as possible small molecule spin labels. *J. Am. Chem. Soc.* **1972**, *94*, 7049–7059. [[CrossRef](#)]
30. Tretyakov, E.V.; Ovcharenko, V.I. The chemistry of nitroxide radicals in the molecular design of magnets. *Russ. Chem. Rev.* **2009**, *78*, 971–1012. [[CrossRef](#)]
31. Rowland, R.S.; Taylor, R. Intermolecular nonbonded contact distances in organic crystal structures: Comparison with distances expected from van der Waals Radii. *J. Phys. Chem.* **1996**, *100*, 7384–7391. [[CrossRef](#)]
32. Swank, D.D.; Landee, C.P.; Willett, R.D. Crystal structure and magnetic susceptibility of copper (II) chloride tetramethylsulfoxide [CuCl₂(TMSO)] and copper (II) chloride monodimethylsulfoxide [CuCl₂(DMSO)]: Ferromagnetic spin- $\frac{1}{2}$ Heisenberg linear chains. *Phys. Rev. B* **1979**, *20*, 2154–2162. [[CrossRef](#)]
33. Baker, G.A.; Rushbrooke, G.S., Jr.; Gilbert, H.E. High-Temperature Series Expansions for the Spin- $\frac{1}{2}$ Heisenberg Model by the Method of Irreducible Representations of the Symmetric Group. *Phys. Rev.* **1964**, *135*, A1272–A1277. [[CrossRef](#)]
34. Clarke, C.S.; Jornet-Somoza, J.; Mota, F.; Novoa, J.J.; Deumal, M. Origin of the Magnetic Bistability in Molecule-Based Magnets: A First-Principles Bottom-Up Study of the TTTA Crystal. *J. Am. Chem. Soc.* **2010**, *132*, 17817–17830. [[CrossRef](#)]
35. Tolstikov, S.E.; Tretyakov, E.V.; Gorbunov, D.E.; Zhurko, I.F.; Fedin, M.V.; Romanenko, G.V.; Bogomyakov, A.S.; Gritsan, N.P.; Mazhukin, D.G. Reaction of Paramagnetic Synthon, Lithiated 4,4,5,5-Tetramethyl-4,5-dihydro-1H-imidazol-1-oxyl 3-oxide, with Cyclic Aldonitrones of the Imidazole Series. *Chem. Eur. J.* **2016**, *22*, 14598–14604. [[CrossRef](#)] [[PubMed](#)]

